Progress In Electromagnetics Research, PIER 21, 273–292, 1999

RIGOROUS ANALYSIS OF E-/H-PLANE JUNCTIONS IN RECTANGULAR WAVEGUIDES USING FOURIER TRANSFORM TECHNIQUE

H. Jia, K. Yoshitomi, and K. Yasumoto

Department of Computer Science and Communication Engineering
Kyushu University 36,
Fukuoka 812-8581, Japan

1. INTRODUCTION

T-junctions in rectangular waveguides play a very important role in the design of microwave circuits, such as multiplexers, power dividers, directional couplers, filters, and phase shifters in modern communication systems [1–4]. Since the modeling of T-junctions is a classical problem, a variety of purely numerical techniques or analytical and numerical methods have been developed during the past decade. Among them, the mode-matching method is a typical one of analytical and numerical approaches.

A wide range of waveguide junctions has a configuration in which several uniform waveguide sections are connected through a cavity region. The mode-matching method uses the expansions of the fields in the waveguide sections in terms of their normal modes. The expanded fields are matched to those of the cavity region to obtain the modal scattering matrix of the discontinuity. This requires a resonant mode expansion of the cavity fields [4, 5] or the use of dyadic Green's func-

tion in the cavity region [6]. In order to avoid such a sophisticated field analysis of the cavity, various techniques [1, 2, 7, 8] based on equivalent circuit concepts have been incorporated in the mode-matching procedure. The cavity problem with multiapertures is reduced [7] to a superposition of simpler cavity problems by subsequently shorting all apertures but one, to which the field expansions by the normal modes can be applied. This principle has been used to analyze asymmetric series E-plane T-junctions [1] and the magic T-junction [2].

A mode-matching method [3] similar to [7] has been devised to obtain the generalized admittance matrix in closed form for E-/H-plane three- and four-port junctions. Although the method provides an accurate full-wave analysis for rectangular waveguide junctions, it needs a larger number of modes with the optimal number ratio for TE and TM modes in each waveguide port.

In this paper, we present the mode-matching method combined with the Fourier transform technique for analyzing rigorously E-/H-plane multiport junctions in rectangular waveguides. The method has been recently applied [10] to the analysis of E-plane T-junction, H-plane T-junction, and right-angle corner bend. We discuss here its extension to the problem of E-/H-plane cross junctions. In this approach, the multiport junctions are treated as a problem of rectangular apertures located on the E-/H-planes of a main waveguide. The electric and magnetic fields in the main waveguide expressed in terms of Fourier integrals are matched on the apertures to those of arm waveguides expanded in terms of normal modes. The mode-matching procedure is performed in the Fourier transformed domain. This yields a system of linear equations in closed form which relates the modal expansion coefficients in the arm waveguides to the field of initial excitation. The main advantage of the method is that the scattering parameters are calculated at one time by solving matrix equations of relatively small dimensions without the relative convergence problem.

The proposed method is applied to the analyses of the Magic-T junction and an asymmetric E-/H-plane three-port junction. It is shown that the convergence of the numerical solutions is very fast. The results are compared with available numerical and experimental data [2,3]. The good agreement between them confirms the validity of the present method.

2. THEORY

The configuration of an E-/H-plane four-port junction is shown schematically in Figure 1, which consists of three rectangular waveguides. For convenience, the waveguide I extending from the port 4 to the port 1 along the z axis is referred to as the main waveguide, and the waveguides Ⅱ and Ⅲ comprising the ports 2 and 3, respectively, are referred to the arm waveguides. The cross sectional dimensions of the waveguides I, Ⅱ and Ⅲ are $2a \times 2b$, $2a \times 2t$ and $2w \times 2b$, respectively. We assume that the TE_{10} mode expressed by the longitudinal section TM^x waves is incident from the right side end of the main waveguide I. When the left side end of the main waveguide I is short-circuited at $z = 0$, the four-port junction is reduced to an E-/H-plane three-port junction. To treat the problems of the four-port and three-port junctions by the same formulation, we express the electric Hertzian vector of the incident field as follows:

$$\mathbf{\Pi}^{\,e}_{in} = \frac{\hat{x}}{k_0^2} \sin \overline{a}_1 (y + a) \left[e^{j\beta_0 z} + \Gamma e^{-j\beta_0 z} \right] \tag{1}$$

where $\overline{a}_1 = \pi/(2a)$, $\beta_0 = \sqrt{k_0^2 - \overline{a}_1^2}$, $k_0 = \omega\sqrt{\epsilon_0 \mu_0}$ is the wavenumber of free space, $\Gamma = 0$ for the original four-port junction, and $\Gamma = -1$ for the modified three-port junction. The first term in the right-hand side of (1) denotes the original incident wave with a unit amplitude, and the second term with $\Gamma = -1$ gives the reflected wave caused by the short-circuited conductor at $z = 0$. The scattered fields into arm waveguides Ⅱ and Ⅲ are expanded using the normal modes of (TE^y, TM^y) and (TE^x, TM^x) of each waveguide, respectively, as follows:

$$\mathbf{\Pi}^e_{\text{Ⅱ}} = \frac{\hat{y}}{k_0^2} \sum_{m=0}^{\infty} \sum_{n=1}^{\infty} A_{mn} e^{-jk_{mn}(x-b)} \cos \overline{a}_m (y + a) \sin \overline{t}_n (z - d + t) \tag{2}$$

$$\mathbf{\Pi}^h_{\text{Ⅱ}} = \frac{\hat{y}}{k_0^2 Z_0} \sum_{m=1}^{\infty} \sum_{n=0}^{\infty} B_{mn} e^{-jk_{mn}(x-b)} \sin \overline{a}_m (y + a) \cos \overline{t}_n (z - d + t) \tag{3}$$

$$\mathbf{\Pi}^e_{\text{Ⅲ}} = \frac{\hat{x}}{k_0^2} \sum_{m=1}^{\infty} \sum_{n=0}^{\infty} C_{mn} e^{-jg_{mn}(y-a)} \sin \overline{w}_m (z - c + w) \cos \overline{b}_n (x + b) \tag{4}$$

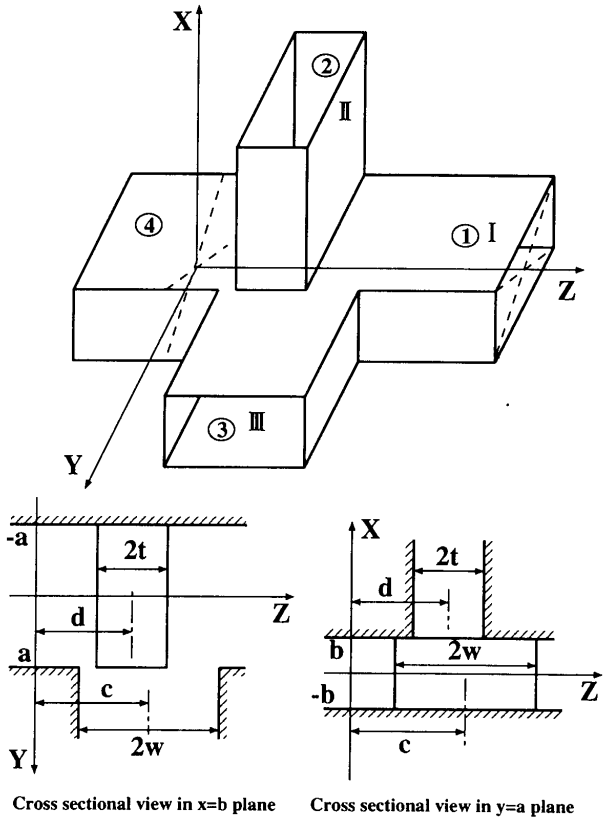

Figure 1. (a) Schematic of an E-/H-plane four-port junction and its cross-sectional views (b) in the plane $x = b$ and (c) in the plane $y = a$.

$$\mathbf{\Pi}_{\mathrm{III}}^{h} = \frac{\hat{x}}{k_0^2 Z_0} \sum_{m=0}^{\infty} \sum_{n=1}^{\infty} D_{mn} e^{-jg_{mn}(y-a)} \cos \overline{w}_m (z - c + w) \cos \overline{b}_n (x + b) \tag{5}$$

where $\overline{a}_m = m\pi/(2a)$, $\overline{w}_m = m\pi/(2w)$, $\overline{b}_n = n\pi/(2b)$, $\overline{t}_n = n\pi/(2t)$, $k_{mn} = \sqrt{k_0^2 - \overline{a}_m^2 - \overline{t}_n^2}$, $g_{mn} = \sqrt{k_0^2 - \overline{w}_m^2 - \overline{b}_n^2}$, $Z_0 = \sqrt{\mu_0/\epsilon_0}$ is the intrinsic impedance of free space, and A_{mn}, B_{mn}, C_{mn} and D_{mn} are unknown expansion coefficients of the transmitted waves.

The Fourier transform technique is used to represent the scattered fields in the main waveguide I. The technique can be directly applied to the problem of the four-port junction with the main waveguide of

an infinite extent in the z direction. For the problem of the three-port junction with the short-circuited conductor at $z = 0$, we introduce an image waveguide structure [10] in $z < 0$ and transform the semi-infinite waveguide I into an infinite uniform waveguide. Using a similar analytical procedure as described in [10], the electric and magnetic Hertzian vectors representing the scattered waves in the main waveguide I are expressed by the Fourier integrals as

$$\begin{aligned}\mathbf{\Pi}_{\mathrm{I}}^{e} = \sum_{\nu=0}^{\infty} \frac{1}{2\pi k_0^2} \int_{-\infty}^{\infty} \Big\{ & \hat{x} A_\nu^e(\zeta) \cos \overline{b}_\nu (x+b) \sin \eta_\nu (y+a) \\ & + \hat{y} B_\nu^e(\zeta) \sin \xi_\nu (x+b) \cos \overline{a}_\nu (y+a) \Big\} e^{-j\zeta z} d\zeta \end{aligned} \tag{6}$$

$$\begin{aligned}\mathbf{\Pi}_{\mathrm{I}}^{h} = \sum_{\nu=0}^{\infty} \frac{1}{2\pi k_0^2 Z_0} \int_{-\infty}^{\infty} \Big\{ & \hat{x} A_\nu^h(\zeta) \sin \overline{b}_\nu (x+b) \\ & + \hat{y} B_\nu^h(\zeta) \cos \xi_\nu (x+b) \sin \overline{a}_\nu (y+a) \Big\} e^{-j\zeta z} d\zeta \end{aligned} \tag{7}$$

where $\eta_\nu = \sqrt{k_0^2 - \overline{b}_\nu^2 - \zeta^2}$, $\xi_\nu = \sqrt{k_0^2 - \overline{a}_\nu^2 - \zeta^2}$, and an infinitesimal small loss has been assumed in the wavenumber k_0 of free space which is finally reduced to zero. In (6) and (7), $A_\nu^e(\zeta)$ and $A_\nu^h(\zeta)$ represent unknown spectral functions for the scattered fields produced by the discontinuity on the E-plane, whereas $B_\nu^e(\zeta)$ and $B_\nu^h(\zeta)$ represent those by the discontinuity on the H-plane. Note that the electric fields derived from (6) and (7) satisfy the boundary conditions on the conducting walls at $x = -b$ and $y = -a$.

The tangential components of electric and magnetic fields derived from (1)–(7) should be continuous across the boundary planes $x = b$ and $y = a$. Taking into account the relations of symmetry [10] of the fields in the original and image waveguides, these boundary conditions may be expressed as follows:

$$E_{\mathrm{I},y}(b,y,z) = \begin{cases} E_{\mathrm{II},y}(b,y,z) & |y| < a, |z-d| < t \\ \Gamma E_{\mathrm{II},y}(b,y,-z) & |y| < a, |z+d| < t \\ 0 & \text{otherwise} \end{cases} \tag{8}$$

$$E_{\mathrm{I},z}(b,y,z) = \begin{cases} E_{\mathrm{II},z}(b,y,z) & |y| < a, |z-d| < t \\ -\Gamma E_{\mathrm{II},z}(b,y,-z) & |y| < a, |z+d| < t \\ 0 & \text{otherwise} \end{cases} \tag{9}$$

$$E_{\mathrm{I},x}(x,a,z) = \begin{cases} E_{\mathrm{III},x}(x,a,z) & |x| < b, |z-c| < w \\ \Gamma E_{\mathrm{III},x}(x,a,-z) & |x| < b, |z+c| < w \\ 0 & \text{otherwise} \end{cases} \tag{10}$$

$$E_{\mathrm{I},z}(x,a,z)=\begin{cases}E_{\mathrm{III},z}(x,a,z) & |x|<b,|z-c|<w\\ -\Gamma E_{\mathrm{III},z}(x,a,-z) & |x|<b,|z+c|<w\\ 0 & \text{otherwise}\end{cases} \tag{11}$$

$$H_{\mathrm{II},y}(b,y,z)=H_{\mathrm{I},y}(b,y,z)+H_{in,y}(b,y,z)\quad |y|<a,|z-d|<t \tag{12}$$

$$H_{\mathrm{II},z}(b,y,z)=H_{\mathrm{I},z}(b,y,z)+H_{in,z}(b,y,z)\quad |y|<a,|z-d|<t \tag{13}$$

$$H_{\mathrm{III},x}(x,a,z)=H_{\mathrm{I},x}(x,a,z)+H_{in,x}(x,a,z)\quad |x|<b,|z-d|<w \tag{14}$$

$$H_{\mathrm{III},z}(x,a,z)=H_{\mathrm{I},z}(x,a,z)+H_{in,z}(x,a,z)\quad |x|<b,|z-d|<w \tag{15}$$

where $H_{in,x}$ to $H_{in,z}$ represent the components of magnetic field of the incident wave deduced from (1). The boundary conditions for the electric fields are first applied. From (6) and (2), the y-components of the electric fields on the plane $x=b$ are derived as follows:

$$E_{\mathrm{I},y}(b,y,z)=\sum_{\nu=0}^{\infty}\frac{1}{2\pi k_0^2}\int_{-\infty}^{\infty}B_\nu^e(\zeta)\frac{k_0^2-\overline{a}_\nu^2}{k_0^2}\sin(2b\xi_\nu)\cos\overline{a}_\nu(y+a)e^{-j\zeta z}d\zeta \tag{16}$$

$$E_{\mathrm{II,y}}(b,y,z)=\sum_{m=0}^{\infty}\sum_{n=1}^{\infty}A_{mn}\frac{k_0^2-\overline{a}_m^2}{k_0^2}\cos\overline{a}_m(y+a)\sin\overline{t}_n(z-d+t). \tag{17}$$

Equations (16) and (17) are substituted into the boundary condition (8). Then (8) is integrated from $y=-a$ to $y=a$ after multiplying both sides by the trigonometric functions $\cos\overline{a}_\mu(y+a)$, where μ is nonnegative integer. The Fourier transform of the resulting expression is calculated with respect to z- coordinate. This leads to an equation which relates the unknown spectral function $B_\mu^e(\zeta)$ to the expansion coefficient $A_{\mu n}$ as

$$B_\mu^e(\zeta)=\sum_{n=1}^{\infty}A_{\mu n}\frac{\overline{t}_n\Theta_n(d,t,\zeta)}{\sin(2\xi_\mu b)} \tag{18}$$

where

$$\Theta_n(d,t,\zeta) = U_n(d,t,\zeta) + \Gamma U_n(d,t,-\zeta) \tag{19}$$

$$U_n(d,t,\zeta) = \frac{e^{j\zeta d}\left[(-1)^n e^{j\zeta t} - e^{-j\zeta t}\right]}{\zeta^2 - \overline{t}_n^2}. \tag{20}$$

The z-component of electric fields derived from (2), (3),(6) and (7) are substituted into the boundary condition (9), and the similar procedure described above is applied to obtain the following relation:

$$B_\mu^h(\zeta) = \sum_{n=0}^{\infty} B_{\mu n} \frac{k_{\mu n}\zeta\Theta_n(d,t,\zeta)}{\xi_\mu \sin(2\xi_\mu b)} \tag{21}$$

The boundary conditions (10) and (11) are applied in a similar way. The x- and z-components of the electric fields derived from (4)–(7) are substituted into (10) and (11), respectively. For this case, the trigonometric functions $\cos\overline{b}_\mu(x+b)$ are multiplied, and (10) and (11) are integrated from $x=-b$ to $x=b$. The Fourier transforms of the resulting expressions lead to the equations which relate the spectral functions $A_\mu^e(\zeta)$ and $A_\mu^h(\zeta)$ to the expansion coefficients $C_{m\mu}$ and $D_{m\mu}$, respectively, as follows:

$$A_\mu^e(\zeta) = \sum_{m=1}^{\infty} C_{m\mu} \frac{\overline{w}_m \Theta_m(c,w,\zeta)}{\sin(2\eta_\mu a)} \tag{22}$$

$$A_\mu^h(\zeta) = \sum_{m=0}^{\infty} D_{m\mu} \frac{g_{m\mu}\zeta\Theta_m(c,w,\zeta)}{\eta_\mu \sin(2\eta_\mu a)}. \tag{23}$$

Next, the boundary conditions (12)–(15) for the magnetic fields are applied. From (1)–(7), the y-components of the magnetic fields on the plane $x=b$ are given by

$$\begin{aligned} &H_{\mathrm{I},y}(b,y,z) \\ &\quad= \sum_{\nu=0}^{\infty} \frac{(-1)^\nu}{2\pi Z_0} \int_{-\infty}^{\infty} \left[\frac{\zeta}{k_0} A_\nu^e(\zeta) - \frac{\overline{b}_\nu \eta_\nu}{k_0^2} A_\nu^h(\zeta)\right] \sin\eta_\nu(y+a) e^{-j\zeta z} d\zeta \\ &\qquad+ \sum_{\nu=0}^{\infty} \frac{1}{2\pi Z_0} \int_{-\infty}^{\infty} \frac{k_0^2 - \zeta^2}{k_0^2} B_\nu^h(\zeta) \cos(2b\xi_\nu) \sin\overline{a}_\nu(y+a) e^{-j\zeta z} d\zeta \end{aligned} \tag{24}$$

$$H_{in,y}(b,y,z) = -\frac{\beta_0}{Z_0 k_0}\sin\overline{a}_1(y+a)\left[e^{j\beta_0 z} - \Gamma e^{-j\beta_0 z}\right] \tag{25}$$

$$H_{\mathrm{II},y}(b,y,z) = \sum_{m=1}^{\infty}\sum_{n=1}^{\infty} B_{mn}\frac{k_0^2 - \overline{a}_m^2}{Z_0 k_0^2}\sin\overline{a}_m(y+a)\cos\overline{t}_n(z-d+t). \tag{26}$$

Equations (24)–(26) are substituted into the boundary condition (12), and the unknown spectral functions $A_\nu^e(\zeta)$, $A_\nu^h(\zeta)$, and $B_\nu^h(\zeta)$ are replaced by the series of the modal expansion coefficients given by (18)–(23). Then (12) is integrated over $|y| \le a$ and $|z-d| \le t$ after multiplying both sides by the trigonometric functions $\sin\overline{a}_p(y+a)\cos\overline{t}_q(z-d+t)$, where p and q are nonnegative integers. This leads to a set of linear equations for the expansion coefficients B_{mn}, C_{mn}, and D_{mn} as follows:

$$\begin{aligned}\frac{k_0^2-\overline{a}_p^2}{k_0^2}B_{pq}t(1+\delta_{q0}) &= -\frac{j(k_0^2-\overline{a}_p^2)}{k_0^2}\sum_{n=0}^{\infty}k_{pn}B_{pn}I_1 - \sum_{m=1}^{\infty}\sum_{n=0}^{\infty}\frac{j(-1)^{p+n}\overline{a}_p\overline{w}_m}{a}C_{mn}I_2 \\ &\quad + \sum_{m=1}^{\infty}\sum_{n=0}^{\infty}\frac{j(-1)^{p+n}\overline{a}_p\overline{b}_n g_{mn}}{k_0 a}D_{mn}I_2 + \frac{j\beta_0^2\delta_{p1}}{k_0}\Theta_q(d,t,\beta_0)\end{aligned} \tag{27}$$

$$\text{for } p = 1,2,\cdots, \quad q = 0,1,2,\cdots$$

with

$$I_1 = \int_{-\infty}^{\infty}\frac{\zeta^2\Theta_n(d,t,\zeta)U_q(d,t,-\zeta)}{2\pi k_0\xi_p\tan(2\xi_p b)}d\zeta \tag{28}$$

$$I_2 = \int_{-\infty}^{\infty}\frac{\zeta^2\Theta_m(c,w,\zeta)U_q(d,t,-\zeta)}{2\pi k_0(\eta_n^2-\overline{a}_p^2)}d\zeta \tag{29}$$

where δ_{mn} denotes the Kronecker's delta. The integrals in (28) and (29) are evaluated in closed form by a simple residue-calculus (See Appendix). Applying the same procedure as described above to (13), we have another set of linear equations:

$$\left[\frac{k_{pq}}{k_0}A_{pq} - \frac{\overline{a}_p\overline{t}_q}{k_0^2}B_{pq}\right] t(1+\delta_{p0})$$
$$= (1+\delta_{p0})\sum_{n=1}^{\infty} j\overline{t}_n\overline{t}_q A_{pn}I_3 - j(1+\delta_{p0})\sum_{n=0}^{\infty}\frac{\overline{a}_p\overline{t}_q k_{pn}}{k_0}B_{pn}I_1$$
$$- \sum_{m=1}^{\infty}\sum_{n=0}^{\infty}\frac{j(-1)^{n+p}\overline{w}_m\overline{t}_q}{a}C_{mn}I_4 - \sum_{m=1}^{\infty}\sum_{n=0}^{\infty} j(-1)^{n+p}\frac{g_{mn}\overline{b}_n\overline{t}_q}{k_0 a}D_{mn}I_2$$
$$- \frac{j\overline{a}_1\beta_0\delta_{p1}}{k_0}\Theta_q(d,t,\beta_0) \tag{30}$$
$$\text{for} \quad p = 0,1,2,\cdots, \quad q = 1,2,\cdots$$

where

$$I_3 = \int_{-\infty}^{\infty}\frac{\xi_p\Theta_n(d,t,\zeta)U_q(d,t,-\zeta)}{2\pi k_0\tan(2\xi_p b)}d\zeta \tag{31}$$
$$I_4 = \int_{-\infty}^{\infty}\frac{\eta_n^2\Theta_m(c,w,\zeta)U_q(d,t,-\zeta)}{2\pi k_0(\eta_n^2-\overline{a}_p^2)}d\zeta. \tag{32}$$

Finally we apply the boundary conditions (14) and (15). The x- and z-components of the magnetic fields on the plane $y = a$ derived from (1)–(7) are substituted into (14) and (15). In this case, (14) and (15) are multiplied by the trigonometric functions $\sin\overline{w}_p(z-c+w)\cos\overline{b}_q(x+b)$ and integrated over $|x| \le b$ and $|z-c| \le w$. Then we have other two sets of equations for the expansion coefficients as follows:

$$\frac{k_0^2-\overline{b}_q^2}{k_0^2}wb(1+\delta_{p0})D_{pq} = \sum_{m=0}^{\infty}\sum_{n=1}^{\infty} j(-1)^{m+q}\overline{b}_q\overline{t}_n A_{mn}J_2$$
$$+ \sum_{m=1}^{\infty}\sum_{n=0}^{\infty} j(-1)^{m+q}\frac{k_{mn}\overline{a}_m\overline{b}_q}{k_0}B_{mn}J_2 - jb\sum_{m=0}^{\infty}\frac{g_{mn}(k_0^2-\overline{b}_q^2)}{k_0}D_{mn}J_1 \tag{33}$$
$$\text{for} \quad p = 0,1,2,\cdots, \quad q = 1,2,\cdots$$

$$\left[\frac{\overline{w}_p\overline{b}_q}{k_0^2}D_{pq}+\frac{g_{pq}}{k_0}C_{pq}\right]wb(1+\delta_{q0})=-\sum_{m=0}^{\infty}\sum_{n=0}^{\infty}j(-1)^{m+q}\overline{t}_n\overline{w}_pA_{mn}J_4$$
$$+\sum_{m=1}^{\infty}\sum_{n=0}^{\infty}j(-1)^{m+q}\frac{k_{mn}\overline{a}_n\overline{w}_p}{k_0}B_{mn}J_2+b(1+\delta_{q0})\sum_{m=1}^{\infty}j\overline{w}_m\overline{w}_pC_{mq}J_3$$
$$+b(1+\delta_{q0})\sum_{m=0}^{\infty}j\frac{g_{mn}\overline{b}_q\overline{w}_p}{k_0}D_{mq}J_1-\frac{2jb\overline{a}_1\overline{w}_p\delta_{q0}}{k_0}\Theta_p(c,w,\beta_0)$$
$$\text{for}\quad p=1,2,\cdots,\quad q=0,1,2,\cdots \tag{34}$$

with

$$J_1=\int_{-\infty}^{\infty}\frac{\zeta^2\Theta_m(c,w,\zeta)U_p(c,w,-\zeta)}{2\pi k_0\eta_q\tan(2\eta_q a)}d\zeta \tag{35}$$

$$J_2=\int_{-\infty}^{\infty}\frac{\zeta^2\Theta_n(d,t,\zeta)U_p(c,w,-\zeta)}{2\pi k_0(\xi_m^2-\overline{b}_q^2)}d\zeta \tag{36}$$

$$J_3=\int_{-\infty}^{\infty}\frac{\eta_q\Theta_m(c,w,\zeta)U_p(c,w,-\zeta)}{2\pi k_0\tan(2\eta_q a)}d\zeta \tag{37}$$

$$J_4=\int_{-\infty}^{\infty}\frac{\xi_m^2\Theta_n(d,t,\zeta)U_p(c,w,-\zeta)}{2\pi k_0(\xi_m^2-\overline{b}_q^2)}d\zeta \tag{38}$$

where J_1 to J_4 denote the integrals characterizing the junction in H-plane and are the counterpart of I_1 to I_4 defined by (28), (29), (31) and (32) for the junction in E-plane. The integrals in (35)–(38) are easily evaluated in closed form by a residue-calculus, though the details have been omitted.

Equations (27), (30), (33) and (34) are solved to obtain the unknown expansion coefficients A_{mn} to D_{mn} for the scattered waves into waveguide Ⅱ and Ⅲ, after truncating the modal expansion up to $m=n=M$. The results are used in (18) and (21)–(23) to determine the unknown spectral functions $B_\mu^e(\zeta)$ to $A_\mu^h(\zeta)$. Using (18) and (21)–(23), the Fourier integrals in (6) and (7) are evaluated in closed form by a simple residue-calculus. The parameter Γ discriminating between the four-port junction and the three-port junction is included in the function $\Theta_n(d,t,\zeta)$ defined by (19). We may take $\Gamma=0$ for the four-port junction and $\Gamma=-1$ for the three-port junction with

a short-circuited conductor at $z = 0$. When the junction is excited by TE_{10} mode incident from waveguide I, the scattering parameters S_{11}, S_{21}, S_{31}, and S_{41} are calculated in terms of expansion coefficients rooted by (27), (30), (33) and (34) as follows:

$$S_{11} = \sum_{m=1}^{M} \frac{-j\overline{a}_1 \overline{w}_m \Theta_m(c, w, \beta_0)}{2a\beta_0} C_{m0} + \sum_{n=0}^{M} \frac{jk_{1n}\beta_0 \Theta_n(d, t, \beta_0)}{4bk_0} B_{1n} \tag{39}$$

$$S_{21} = \sqrt{t/b} B_{10} \tag{40}$$

$$S_{31} = \sqrt{\frac{a(k_0^2 - \overline{w}_1^2)^{\frac{3}{2}}}{w\beta_0 k_0^2}} C_{10} \tag{41}$$

$$S_{41} = \sum_{m=1}^{M} \frac{-j\overline{a}_1 \overline{w}_m U_m(c, w, -\beta_0)}{2a\beta_0} C_{m0} - \sum_{n=1}^{M} \frac{jk_{1n}\beta_0 U_n(d, t, -\beta_0)}{4bk_0} B_{1n}$$
$$\text{only for} \quad \Gamma = 0 \tag{42}$$

The other elements of scattering matrix can be obtained by changing the port of initial excitation.

3. NUMERICAL RESULTS

The proposed Fourier transform technique has been applied to the analysis of a four-port E-/H-plane junction and a three-port E-/H-plane junction. The results have been compared with available numerical and experimental data. The scattering parameters were calculated from (39)–(42). The modal expansions of scattered fields in the arm waveguides Ⅱ and Ⅲ were truncated at $m = n = M$. Then (27), (30), (33), and (34) are rendered into a matrix equation with $4M(M+1)$ unknowns. We first consider the Magic-T which is a junction of four identical waveguides comprising an E-/H-plane T-junction. The values of geometrical parameters in Figure 1 were chosen to be $2a = 2w = 15.799\ mm$ and $2b = 2t = d = c = 7.899\ mm$. Table I shows the convergence of the scattering parameters for $f = 16.5\ GHz$ and the CPU time of computation versus the truncation number M of modal expansions in waveguides Ⅱ and Ⅲ. The numerical computation was run on Sun Ultra 1 (UltraSPARC 143 MHz) workstation. We can see that a very good convergence is achieved for all scattering parameters as the number of modes increases. When the mode number

M	S_{11}	S_{21}	S_{31}	S_{41}	CPU(s)
1	0.097915∠23.79°	0.559953∠−22.89°	0.419174∠−109.64°	0.707925∠17.66°	0.02
2	0.159804∠61.49°	0.565849∠−30.87°	0.436739∠−104.27°	0.680835∠8.00°	0.04
3	0.160002∠60.56°	0.566354∠−30.96°	0.434270∠−104.17°	0.681947∠7.83°	0.12
4	0.163797∠62.27°	0.563544∠−31.26°	0.435297∠−103.77°	0.682719∠7.21°	0.33
5	0.164247∠61.83°	0.563675∠−31.28°	0.433320∠−103.86°	0.683759∠7.18°	0.79
6	0.165319∠62.44°	0.562450∠−31.37°	0.433650∠−103.73°	0.684301∠6.99°	1.62
7	0.165565∠62.23°	0.562507∠−31.38°	0.432634∠−103.79°	0.684837∠6.98°	3.50
8	0.166167∠62.49°	0.562027∠−31.41°	0.432788∠−103.73°	0.684989∠6.88°	6.62
9	0.166295∠62.42°	0.562058∠−31.42°	0.432409∠−103.75°	0.685171∠6.88°	12.70
10	0.166698∠62.56°	0.561845∠−31.44°	0.432496∠−103.71°	0.685193∠6.82°	21.69
11	0.166787∠62.52°	0.561864∠−31.44°	0.432258∠−103.72°	0.685306∠6.82°	37.73
12	0.167047∠62.61°	0.561709∠−31.45°	0.432312∠−103.70°	0.685335∠6.79°	62.49
13	0.167112∠62.58°	0.561722∠−31.46°	0.432121∠−103.71°	0.685430∠6.79°	97.46
14	0.167281∠62.64°	0.561601∠−31.46°	0.432158∠−103.69°	0.685464∠6.76°	153.41
15	0.167330∠62.62°	0.561610∠−31.47°	0.432010∠−103.70°	0.685538∠6.76°	237.35

Table I. Convergence of the magnitude and phase of scattering parameters at $f = 16.5\ GHz$ versus the truncation number M of modal expansion for a Magic T-junction with $2a = 2w = 15.799\ mm$ and $2b = 2t = c = d = 7.899\ mm$.

is truncated at $M = 4$, the relative errors of the solutions are about 2% for $|S_{11}|$ and less than 1% for $|S_{21}|$, $|S_{31}|$, and $|S_{41}|$. It is worth noting that the results given in Table I satisfy accurately the energy conservation relation $\sum_{i=1}^{4} |S_{i1}|^2 = 1$ for any truncation of modal expansion. Figure 2 illustrates $|S_{11}|$, $|S_{21}|$, $|S_{31}|$, and $|S_{41}|$ as functions of frequency for different numbers of modes used in the analysis. The scattering parameters converge very fast and no significant difference is observed between the results for $M = 4$ and for $M = 6$. Note that the total number of modes used is 80 when $M = 4$. The same structure has been analyzed [3] by using the generalized admittance matrix approach. For the sake of comparison, the numerical results of $|S_{11}|$ given in [3] are reproduced in Figure 3. The curves indicated by the labels a, b, c, d, e, and f were obtained by using 19, 24, 28, 38, 45, and 60 modes in each of four ports, respectively. It follows that the generalized admittance matrix approach requires the total 180 modes at least to obtain the stable and convergent results. Comparing Figure 2(a) with Figure 3, it is seen that the total mode numbers used in

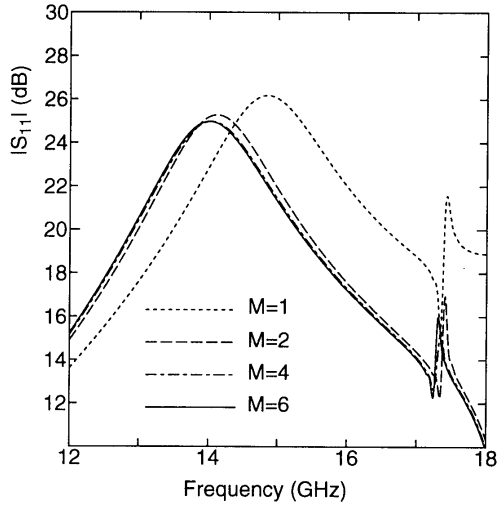

Figure 2a

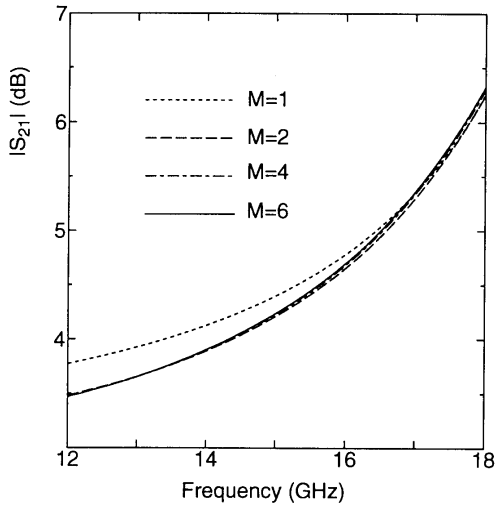

Figure 2b

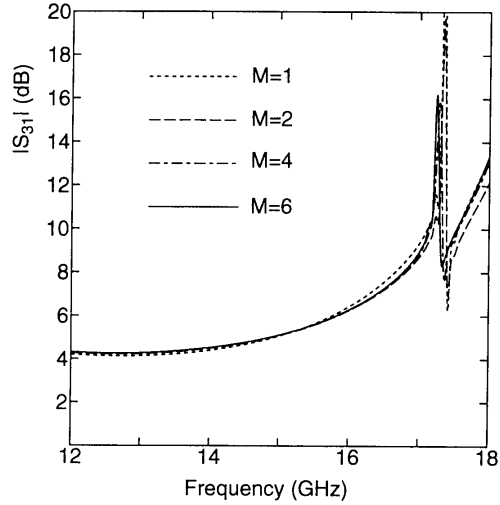

Figure 2c

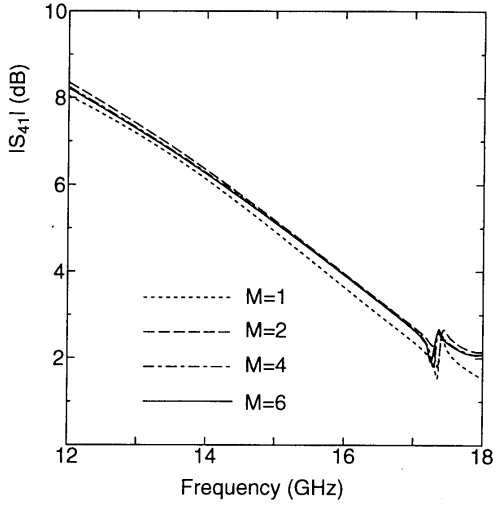

Figure 2d

Figure 2. Magnitudes of the scattering parameters for a Magic-T junction with $2a = 2w = 15.799\ mm$ and $2b = 2t = c = d = 7.899\ mm$ for the different truncation number M of modal expansion; (a) $|S_{11}|$, (b) $|S_{21}|$, (c) $|S_{31}|$, (d) $|S_{41}|$. The total number of modes used in the analysis is $4M(M+1)$ for each of M.

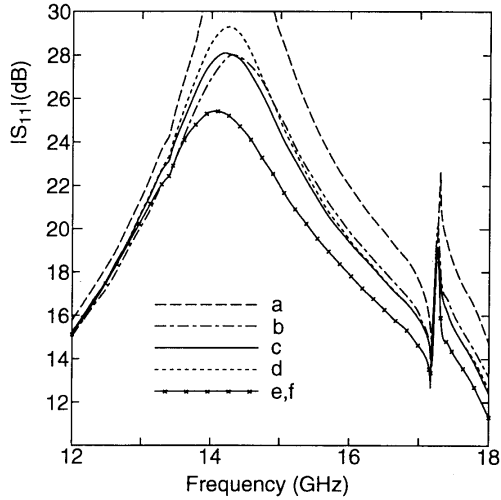

Figure 3. Scattering parameter $|S_{11}|$ calculated using the generalized admittance matrix approach for the same Magic-T junction as shown in Figure 2. The results have been reproduced from Fig. 12(a) of reference [3]. The number of modes used in each of four ports are 19, 24, 28, 38, 45, and 60 for the curves a, b, c, d, e, and f, respectively.

the present method is far less than that of the generalized admittance matrix approach to obtain the same accuracy. Another important difference is in the relative convergence problem. For the generalized admittance matrix approach, there exists an optimal ratio [3] between the number of TE and TM modes used to achieve a faster and stable convergence. We have never observed such a situation for the present method. Using the Fourier integral representation of fields in the main waveguide I, the modal expansion coefficients in two arm-waveguides II and III have been directly related through the algebraic equations (27), (30), (33), and (34). This reduces the number of unknowns to be determined and removes the problem of relative convergence.

Figure 4 shows the numerical results of the magnitudes of the scattering parameters for the Magic-T with $2a = 2w = 22.86\ mm$, $2b = 2t = 10.16\ mm$, and $c = d = 11.43\ mm$. The results are compared with the measured data [2]. For the analysis of $|S_{22}|$ and $|S_{33}|$ in Figure 4(b), we have changed the port of initial excitation. It is seen that the present results agree very well with the measured one.

We consider next an asymmetric E-/H-plane three-port junction. The magnitudes of scattering parameters of the junction with $2a =$

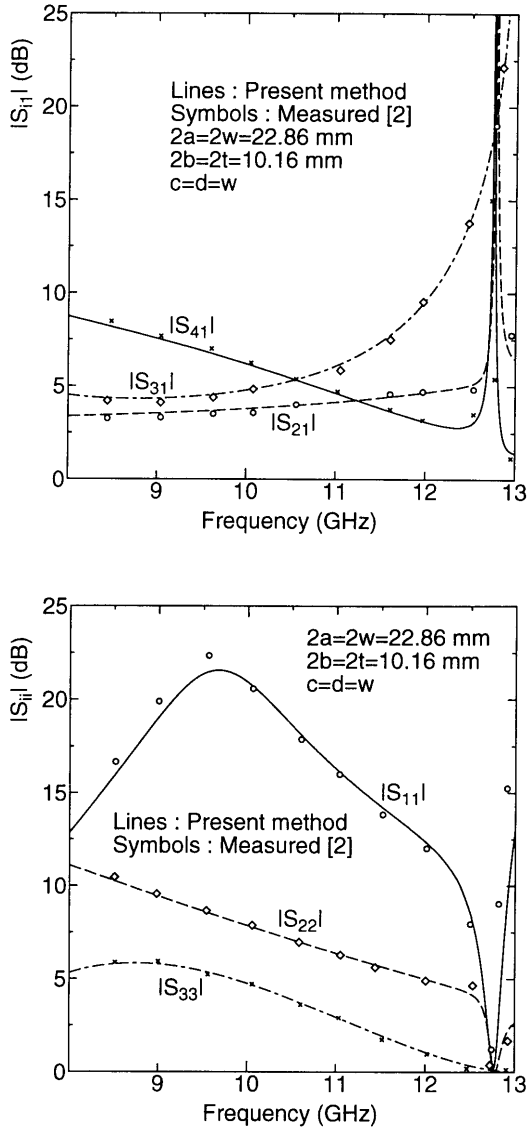

Figure 4. Magnitude of the scattering parameters for a Magic-T junction with $2a = 2w = 22.86\ mm$, $2b = 2t = 10.16\ mm$, and $c = d = 11.43\ mm$.

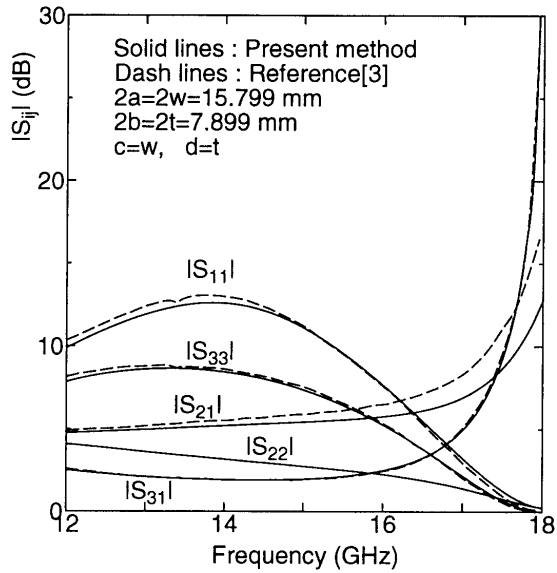

Figure 5. Magnitude of the scattering parameters for an asymmetric E-/H-plane three-port junction with $2a = 2w = 15.799\ mm$, $2b = 2t = 2d = c = 7.899\ mm$. The left side end of waveguide I in Figure 1 is short-circuited at $z = 0$.

$2w = 15.799\ mm$ and $2b = 2t = 2d = c = 7.899\ mm$ are plotted in Figure 5 for the excitation of each of three ports, and are compared with those [3] obtained by the generalized admittance matrix approach using 28 modes in each of ports. We note that both results are in good agreement. A small discrepancy is observed in $|S_{11}|$ and $|S_{21}|$, since the number of modes used in [3] was not sufficient for the accurate computation.

4. CONCLUSION

A rigorous and efficient technique for the analysis of a rectangular waveguide E-/H-plane junction has been presented. The approach is a combination of the Fourier transform technique and the mode-matching method. By introducing an idea of image waveguide, the problem of the junction was transformed into a problem of rectangular apertures located on the E-/H-planes of the main waveguide of infinite extent. When the Fourier transform technique is applied to the fields

of the main waveguide, a set of linear equations relating the amplitudes of the normal mode expansion in each of arm waveguides are obtained in analytically closed form. This technique reduces significantly the number of unknowns to be determined and removes the problem of relative convergence. The scattering parameters can be calculated by solving a matrix equation of relatively small dimension. The numerical results of the scattering parameters calculated for the Magic-T junction and an asymmetric E-/H-plane three-port junction were in a very good agreement with the available numerical and experimental data.

APPENDIX

Using the residue-calculus, the integral in (28) is evaluated as follows:

$$I_1 = -\frac{t(1+\delta_{n0})\delta_{nq}}{k_0 k_{pn}\tan(2k_{pn}b)} - j\sum_{\nu=0}^{\infty}\frac{\zeta_{p\nu}\left[1-(-1)^{n+q}e^{-j2\zeta_{p\nu}t}\right]Q_{qn}}{k_0 b(1+\delta_{\nu 0})(\zeta_{p\nu}^2-\overline{t}_n^2)(\zeta_{p\nu}^2-\overline{t}_q^2)} + j\sum_{\nu=0}^{\infty}\Gamma\frac{\zeta_{p\nu}\left[(-1)^{n+q}e^{-j2\zeta_{p\nu}t}+e^{2j\zeta_{p\nu}t}-(-1)^n-(-1)^q\right]e^{-j2\zeta_{p\nu}d}}{2bk_0(1+\delta_{\nu 0})(\zeta_{p\nu}^2-\overline{t}_n^2)(\zeta_{p\nu}^2-\overline{t}_q^2)} \tag{A1}$$

with

$$Q_{qn} = \begin{cases} 1 & q+n \stackrel{\triangle}{=} \text{even} \\ 0 & q+n \stackrel{\triangle}{=} \text{odd} \end{cases} \tag{A2}$$

where $k_{pn} = \sqrt{k_0^2 - \overline{a}_p^2 - \overline{b}_n^2}$ and $\zeta_{p\nu} = \sqrt{k_0^2 - \overline{a}_p^2 - \overline{b}_\nu^2}$. The first term in (A1) is calculated from the residues at $\zeta = \pm\overline{t}_n$, the second term is from the residues at $\zeta = \pm\zeta_{p\nu}$ which satisfy $\tan(2\xi_p b) = 0$, and the third term is from the residues at $\zeta = \zeta_{p\nu}$. It is easy to show that the poles of the integrand in (28) located at $\zeta = \pm\overline{t}_n$ and at $\zeta = -\zeta_{p\nu}$ have no contribution to the result of the integration for a finite value

of Γ. Similarly, the integral in (29) is evaluated as follows:

$$
\begin{aligned}
I = & \frac{\Big(j\zeta_{pn}e^{-j\zeta_{pn}w}\left[(-1)^q e^{j\zeta_{pn}t} - e^{-j\zeta_{pn}t}\right] \times \\
& \qquad \left[(-1)^m e^{-j\zeta_{pn}(c-d)} + (-1)^q e^{j\zeta_{pn}(c-d)}\right]\Big)}{2k_0(\zeta_{pn}^2 - \overline{w}_m^2)(\zeta_{pn}^2 - \overline{t}_q^2)} \\
& - j\Gamma \frac{e^{-j\zeta_{pn}(c+d)}\zeta_{pn}\left[(-1)^m e^{-j\zeta_{pn}w} - e^{j\zeta_{pn}w}\right]\left[(-1)^q e^{-j\zeta_{pn}t} - e^{j\zeta_{pn}t}\right]}{2k_0(\zeta_{pn}^2 - \overline{w}_m^2)(\zeta_{pn}^2 - \overline{t}_q^2)} \\
& - \frac{\Big(j\overline{w}_m e^{-j\overline{w}_m w}\left[(-1)^q e^{j\overline{w}_m t} - e^{-j\overline{w}_m t}\right] \times \\
& \qquad \left[(-1)^q e^{j\overline{w}_m(c-d)} + (-1)^m e^{-j\overline{w}_m(c-d)}\right]\Big)}{2k_0(g_{mn}^2 - \overline{a}_p^2)(\overline{w}_m^2 - \overline{t}_q^2)}
\end{aligned}
\tag{A3}
$$

where $\zeta_{pn} = \sqrt{k_0^2 - \overline{a}_p^2 - \overline{b}_n^2}$ and $g_{mn} = \sqrt{k_0^2 - \overline{w}_m^2 - \overline{b}_n^2}$. The first and second terms in (A3) are calculated from the residues at $\zeta = \pm\zeta_{pn}$ and the third term is from the residues at $\zeta = \pm\overline{w}_m$. The poles of the integrand in (29) at $\zeta = \pm\overline{t}_n$ has no contribution to the result of the integration. The integrals in I_3, I_4, and J_1 to J_4 defined by (31), (32), and (35) to (38) are evaluated in closed form using the similar residue-calculus.

REFERENCES

1. Arndt, F., I. Ahrens, U. Papziner, U. Wiechmann, and R. Willkeit, "Optimized E-plane T-junction series power dividers," *IEEE Trans. Microwave Theory Tech.,* Vol. MTT-35, 1052–1059, 1987.
2. Sieverding, T. and F. Arndt, "Modal analysis of the magic Tee," *IEEE Microwave and Guide Wave Lett.,* Vol. 3, 150–152, 1993.
3. Rebollar, J. M., J. Esteban, and J. E. Page, "Fullwave analysis of three and four-port rectangular waveguide junctions," *IEEE Trans. Microwave Theory Tech.,* Vol. MTT-42, 256–263, 1994.
4. Alessandri, F., M. Mongiardo, and R. Sorrentino, "Computer-aided design of beam forming networks for modern satellite antennas," *IEEE Trans. Microwave Theory Tech.,* Vol. 40, 1117–1127, 1992.

5. Alessandri, F., M. Mongiardo, and R. Sorrentino, "Rigorous mode matching analysis of mitered E-plane bends in rectangular waveguide," *IEEE Microwave and Guide Wave Lett.,* Vol. 4, 408–410,1994.
6. Alessandri, F., M. Mongiardo, and R. Sorrentino, "A technique for the fullwave automatic synthesis of waveguide components: application to fixed phase shifters," *IEEE Trans. Microwave Theory Tech.,* Vol. 40, 1484–1495, 1992.
7. Kühn, E., "A mode-matching method for solving field problem in waveguide and resonator circuits," *Arch. Elek. Übertragung.,* Vol. 27, 511–518, 1973.
8. Sieverding, T. and F. Arndt, "Field theoretic CAD of open or aperture matched T-junction coupled rectangular waveguide structures," *IEEE Trans. Microwave Theory Tech.,* Vol. 40, 353–362, 1992.
9. Mittra, R. and S. W. Lee, *Analytical Techniques in the Theory of Guided Waves,* New York: Macmillan Co., 1971.
10. Jia, H., K. Yoshitomi, and K. Yasumoto, "Rigorous analysis of rectangular waveguide junctions by Fourier transform technique," *Progress in Electromagnetics Research,* PIER 20, 261–280, 1998.